On the Origin of Density Cusps in Elliptical Galaxies

Taro Nakano and Junichiro Makino

Department of General Systems Studies, College of Arts and Sciences, University of Tokyo, 3-8-1 Komaba, Meguro-ku, Tokyo 153, Japan

ABSTRACT

We investigated the dynamical reaction of the central region of galaxies to a falling massive black hole by N-body simulations. As the initial galaxy model, we used an isothermal King model and placed a massive black hole at around the half-mass radius of the galaxy. We found that the central core of the galaxy is destroyed by the heating due to the black hole and that a very weak density cusp ($\rho \propto r^{-\alpha}$, with $\alpha \sim 0.5$) is formed around the black hole. This result is consistent with recent observations of large elliptical galaxies with *Hubble Space Telescope*. The velocity of the stars becomes tangentially anisotropic in the inner region, while in the outer region the stars have radially anisotropic velocity dispersion. The radius of the weak cusp region is larger for larger black hole mass. Our result naturally explains the formation of the weak cusp found in the previous simulations of galaxy merging, and implies that the weak cusp observed in large elliptical galaxies may be formed by the heating process by sinking black holes during merging events.

Subject headings: galaxies: elliptical and lenticular, cD — galaxies: kinematics and dynamics — galaxies: nuclei — galaxies: structure — methods: numerical

1. Introduction

Recent *HST* observations (Lauer et al. 1995; Byun et al. 1996; Gebhardt et al. 1996; Faber et al. 1996; Kormendy et al. 1996) have drastically changed our understanding of the structure of elliptical galaxies. First, no elliptical galaxies have cores with constant surface brightness. All of them turned out to have cusps with power-law surface brightness profiles. Second, elliptical galaxies are divided into two groups in terms of the slope of the cusp: "weak-cusp" galaxies and "strong-cusp" galaxies. The weak-cusp galaxies have the surface brightness profiles expressed as $I(R) \propto R^{-\gamma}$ with $0 \lesssim \gamma \lesssim 0.3$ and deprojected luminosity density profiles expressed as $\rho(r) \propto r^{-\alpha}$ with $0.3 \lesssim \alpha \lesssim 1.1$ (Kormendy et al. 1996). On the other hand, the cusps of the strong-cusp galaxies are expressed by the same formula, but with $\gamma \simeq 1$ and $\alpha \simeq 2$. In addition, it was found that bright galaxies have weak cusps, while faint galaxies have strong cusps.

Previously, bright elliptical galaxies were believed to have cores with constant surface brightness. High-resolution surface photometry showed that these cores are non-isothermal (Lauer 1985; Kormendy 1985). *HST* observations revealed these cores are actually weak cusps.

The origin of such weak cusps is not well understood. One possible way to form a density cusp is to introduce the central black hole. Young (1980) studied the response of the structure of a stellar system to the adiabatic growth of the central black hole. He showed that the power-law density cusp with $\rho \propto r^{-3/2}$ is formed around the black hole. The same result was obtained by Quinlan, Hernquist, & Sigurdsson (1995).

Another way to form cusps using a central black hole was proposed by Bahcall & Wolf (1976). They investigated the evolution of the structure of a stellar system around a black hole driven by two-body relaxation. They found a steady state solution with a steep cusp. Shapiro & Marchant (1978) and Marchant & Shapiro (1979, 1980) performed Monte Carlo simulation and found that this steady state cusp is actually formed.

Both models predict cusps steeper than the observed ones. Therefore the origin of these weak cusps cannot be explained by means of these mechanisms.

Navarro, Frenk, & White (1996) found that the dark matter halos formed in standard CDM cosmogony is well approximated by a "universal profile" which approaches $\rho \propto r^{-1}$ near the center. They argued that this result might explain the origin of weak cusps. Recently, Fukushige & Makino (1997) performed the same calculation as Navarro et al. (1996), but with much higher resolution in both mass and space. They obtained a nearly isothermal cusp. Thus the cusps formed by CDM clustering scenario are also too steep.

So far, the only scenario that successfully reproduced the weak cusps is the merging of two galaxies with central black holes (Makino & Ebisuzaki 1996, hereafter ME). They investigated the mergings of two galaxies with central black holes by N-body simulations and found that the merger remnants have very shallow ($\rho \propto r^{-1}$ or shallower) density cusps in the central regions. This result is in good agreement with the *HST* observations.

The physical process by which the weak cusps are formed in a merger remnant was not clearly explained in ME. It is obvious that the black holes played some important roles in the cusp formation, since no significant cusps were formed by the merger remnant of two galaxies without black holes. The merging of two galaxies with black holes involves several processes, such as the sinking of two black holes to the center of the remnant due to dynamical friction from field stars, the formation and hardening of a black hole binary and its back reaction to field stars. We need simpler models with which we can study the effect of each elementary process separately.

In the present work, we study the sinking of a black hole due to dynamical friction and its back reaction to the distribution of field stars. We performed N-body simulation of the system of spherical galaxy model and a black hole placed at around the half mass radius of the galaxy. We found the shallow density cusp with $\rho \sim r^{-0.5}$ is formed in the center of galaxies. Thus we can conclude that the sinking of black hole is the dominant mechanism of the formation of weak cusps.

In the next section, we describe the numerical methods and initial models we used. We present our results in §3 and a discussion and summary in §4.

2. Initial Conditions and Numerical Method

2.1. Initial Conditions

The initial conditions we used are summarized in Table 1. Column 2 shows the initial galaxy models.

We used King models with the central potential parameter $W_c = 9$, 6 and 3 as initial galaxy models. The number of particles in the initial galaxies (column 3) was 32767 or 131071, and all particles have equal mass. We adopted the standard unit (Heggie & Mathieu 1986) as the system of units, in which $G = M_{\rm gal} = 1$ and $E_{\rm gal} = -1/4$, where G is the gravitational constant, $M_{\rm gal}$ is the total mass of the initial galaxy and $E_{\rm gal}$ is the total energy of the galaxy. In these units, the half-mass radii of the initial galaxies are 0.98, 0.80 and 0.84 for the King models with $W_c = 9$, 6 and 3, respectively. The half-mass crossing time is $2\sqrt{2}$ for all models. Column 4 shows the black hole masses. We used different black hole masses (2, 4, 8 % of the mass of the whole system). Column 5 shows the initial position and velocity of the black hole. We tried three different set of initial conditions of the black hole. In "off-center" runs (runs A, F, G, H, I and J), we initially placed a black hole in the position of $r = 1$ from the center of mass of the galaxy (Figure 1). In the "spiral-in" runs (run B, C and D), we placed a black hole in the same position as in the off-center runs with some initial tangential velocity v_t. We varied v_t as v_K, $0.5v_K$ and $0.25v_K$, where $v_K = \sqrt{GM(r)/r}\,\Big|_{r=1}$ (circular velocity at the initial position). In the third set, which is the "on-center" run (run E), however, we put the black hole exactly at the center of the galaxy, to compare the result with those of other runs. For both off-center and on-center runs, the initial velocity of the black hole was zero.

2.2. Numerical Method

We used the `NBODY1` calculation code (Aarseth 1985) modified for GRAPE-4, a special-purpose computer for astronomical N-body problem (Taiji et al. 1996). In this code, we used the Hermite scheme (Makino & Aarseth 1992) to carry out time integration of orbits. The equation of motion for star i is given by

$$\frac{d^2\boldsymbol{r}_i}{dt^2} = -\sum_{j\neq i} \frac{Gm_j(\boldsymbol{r}_i - \boldsymbol{r}_j)}{(|\boldsymbol{r}_i - \boldsymbol{r}_j|^2 + \epsilon^2)^{3/2}} \qquad (1)$$

where $\boldsymbol{r}$ and m are the position and mass of the star, respectively, and ϵ is the softening parameter which is added to avoid divergence of the gravitational force between close stars. The softening length is 1/1024 for the force between field star particles and is 10^{-8} for the force between a black hole particle and a field star. These softening parameters are small enough to achieve necessary spatial resolution, since we are interested in the central structure of the scale of $\sim 10^{-2}$ or larger. The maximum relative energy error at the end of the run was 1.079×10^{-4} (for run A) and typical error was 10^{-5} along the calculations. The black hole is represented by a particle that has much larger mass than that of a field particle. The mass accretion to the black hole through tidal disruption of field stars or relativistic effects were not taken into account.

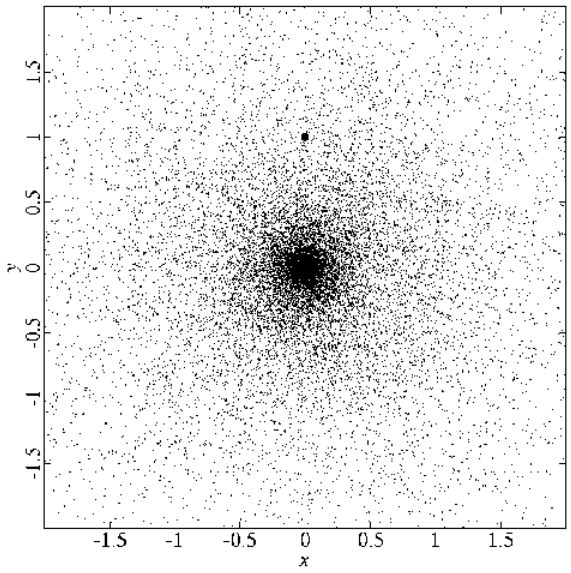

Fig. 1.— The snapshot of the whole system at $t = 0$ for run A. The filled circle on $(x, y) = (0, 1)$ shows the initial position of a massive BH.

3. Results

3.1. Motion of the Black Hole

Figure 2 shows the trajectory of the black hole in the center-of-mass reference frame for the off-center run (run A) and the spiral-in run (run B). The time ranges from $t = 0$ to $t = 10$ for run A and from $t = 0$ to $t = 15$ for run B. In this coordinate system, the massive black hole is initially put on $(x, y, z) = (0, 1, 0)$. In the off-center run (Figure 2a and c), the black hole oscillates around the center of the system and its amplitude is damped quickly due to the dynamical friction of the field stars. In the spiral-in run (Figure 2b), the black hole sinks into the center along the spiral orbit. Even after the os-

TABLE 1
INITIAL CONDITIONS

Run (1)	Galaxy Model (2)	N (3)	$M_{\rm BH}$ (4)	BH Initial Condition (5)
A	King ($W_{\rm c}=9$)	32767	1/24	$r=1$, $v_{\rm t}=0$
B	King ($W_{\rm c}=9$)	32767	1/24	$r=1$, $v_{\rm t}=v_{\rm K}$
C	King ($W_{\rm c}=9$)	32767	1/24	$r=1$, $v_{\rm t}=0.5v_{\rm K}$
D	King ($W_{\rm c}=9$)	32767	1/24	$r=1$, $v_{\rm t}=0.25v_{\rm K}$
E	King ($W_{\rm c}=9$)	32767	1/24	$r=0$
F	King ($W_{\rm c}=9$)	32767	1/49	$r=1$, $v_{\rm t}=0$
G	King ($W_{\rm c}=9$)	32767	2/23	$r=1$, $v_{\rm t}=0$
H	King ($W_{\rm c}=6$)	32767	1/24	$r=1$, $v_{\rm t}=0$
I	King ($W_{\rm c}=3$)	32767	1/24	$r=1$, $v_{\rm t}=0$
J	King ($W_{\rm c}=9$)	131071	1/24	$r=1$, $v_{\rm t}=0$

cillation or spiral motion is damped ($t \gtrsim 5$ for run A and $t \gtrsim 10$ for run B), the black hole moves randomly around the bottom of the potential well, because the random velocity of the black hole reaches equipartition with that of field stars. The typical length scale of this random motion is, from Figure 2c, around 0.01. Thus, we can analyze the system, assuming that the black hole is at the center, up to the radius of 0.01. The all following results in this paper are described on this assumption. The structure smaller than this radius is probably meaningless.

3.2. Density Profiles

Figures 3, 4 and 5 show the spatial and surface density profiles for the off-center run (run A), the spiral-in runs (runs B,C and D), and the on center run (run E). As mentioned in §3.1, we take the position of the black hole as the center of galaxy (and thus as the origin of the coordinate system) in the results of run A for $t \gtrsim 5$ and runs B, C and D for $t \gtrsim 10$. We calculated the surface density $\Sigma(R)$ by summing up the contribution of all stars outside radius R:

$$\begin{aligned}\Sigma(R) &= 2\int_R^\infty \frac{r\rho}{\sqrt{r^2-R^2}}dr \\ &= \frac{1}{2\pi}\sum_{i(r_i>R)}\frac{m_i}{r_i\sqrt{r_i^2-R^2}}, \end{aligned} \quad (2)$$

where r_i and m_i are the distance from the center of the galaxy and the mass of star i, respectively.

In Figure 3, we can see that the central region of the initial King profile was destroyed by the black hole and a very weak cusp of $\rho \propto r^{-0.5}$ is formed. This result is similar to that of ME and in good agreement with the *HST* observations (Lauer et al. 1995; Byun et al. 1996; Gebhardt et al. 1996; Faber et al. 1996; Kormendy et al. 1996). For the spiral-in runs (Figure 4), we obtained the density profiles similar to the off-center run. The central region has $\rho \propto r^{-0.5}$ cusp for all cases. On the other hand, when the black hole is placed initially at the center, the density structure becomes quite different (Figure 5a and b). The cusp in Figure 5a is approximately $\rho \propto r^{-1.5}$.

3.3. Velocity Structure

In Figures 6, 7, 8 and 9, we show the velocity profile, anisotropy and kurtosis.

The projected (line-of-sight) velocity dispersion is calculated using the following formula (Merrifield & Kent 1990):

$$\begin{aligned}\sigma_{\rm los}(R) &= \left\{\frac{2}{\Sigma(R)}\int_R^\infty \frac{dr\, r\rho}{\sqrt{r^2-R^2}}\right. \\ &\quad \left.\times\left[\left(1-\frac{R^2}{r^2}\right)\langle v_r^2\rangle + \frac{1}{2}\frac{R^2}{r^2}\langle v_t^2\rangle\right]\right\}^{1/2} \\ &= \left\{\frac{1}{2\pi\Sigma(R)}\sum_{i(r_i>R)}\frac{m_i}{r_i\sqrt{r_i^2-R^2}}\right.\end{aligned}$$

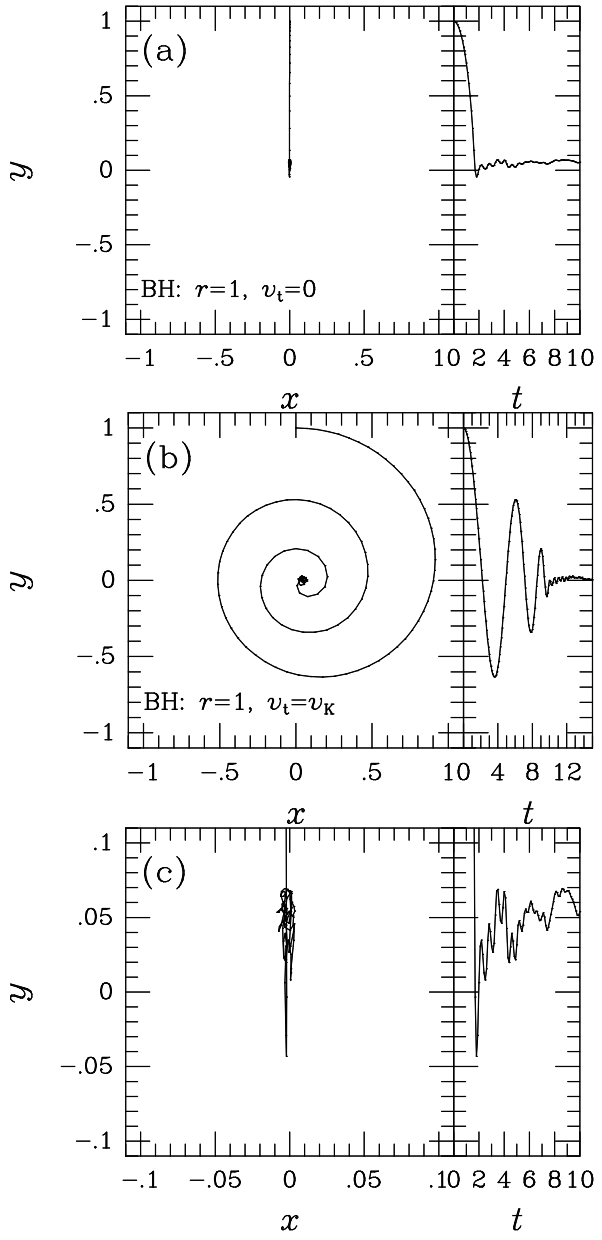

Fig. 2.— (a) Left: Trajectory of a BH on $x-y$ plane for $t = 0-10$ for off-center BH (run A); Right: Time evolution of the y-component of the BH's position. (b) Same as (a) but for spiral-in BH (run B). (c) 10 times magnified view of the central region of (a).

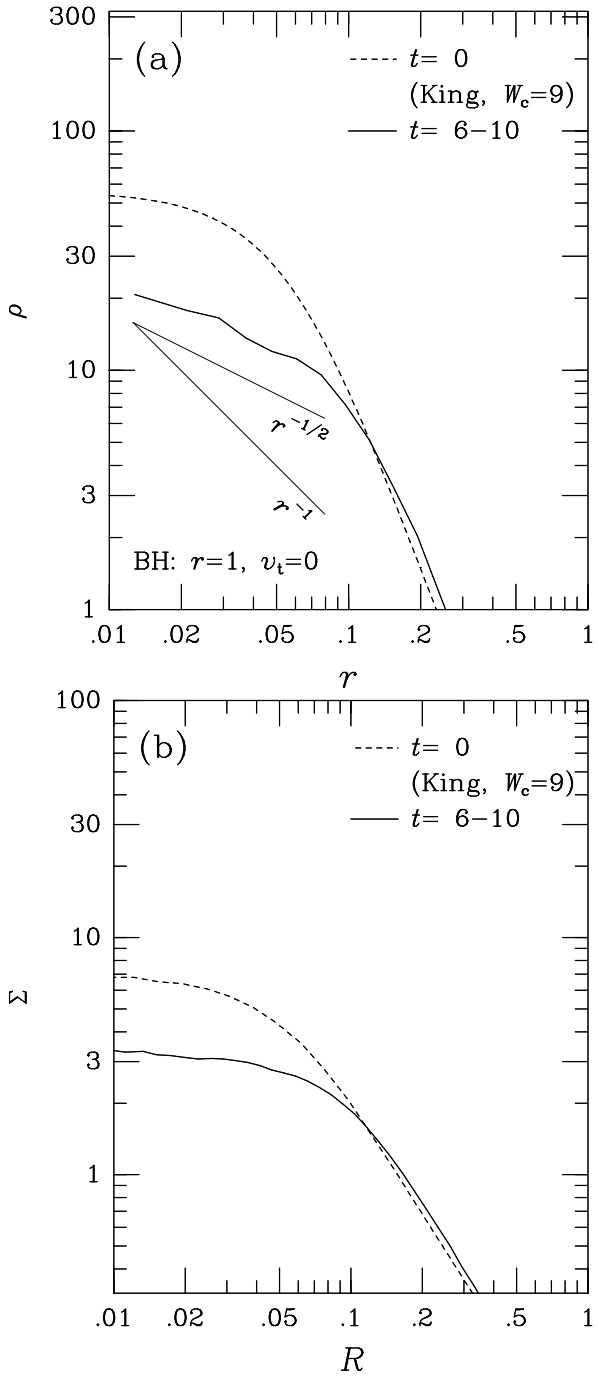

Fig. 3.— Results for off-center BH (run A): (a) density profile; (b) surface density profile.

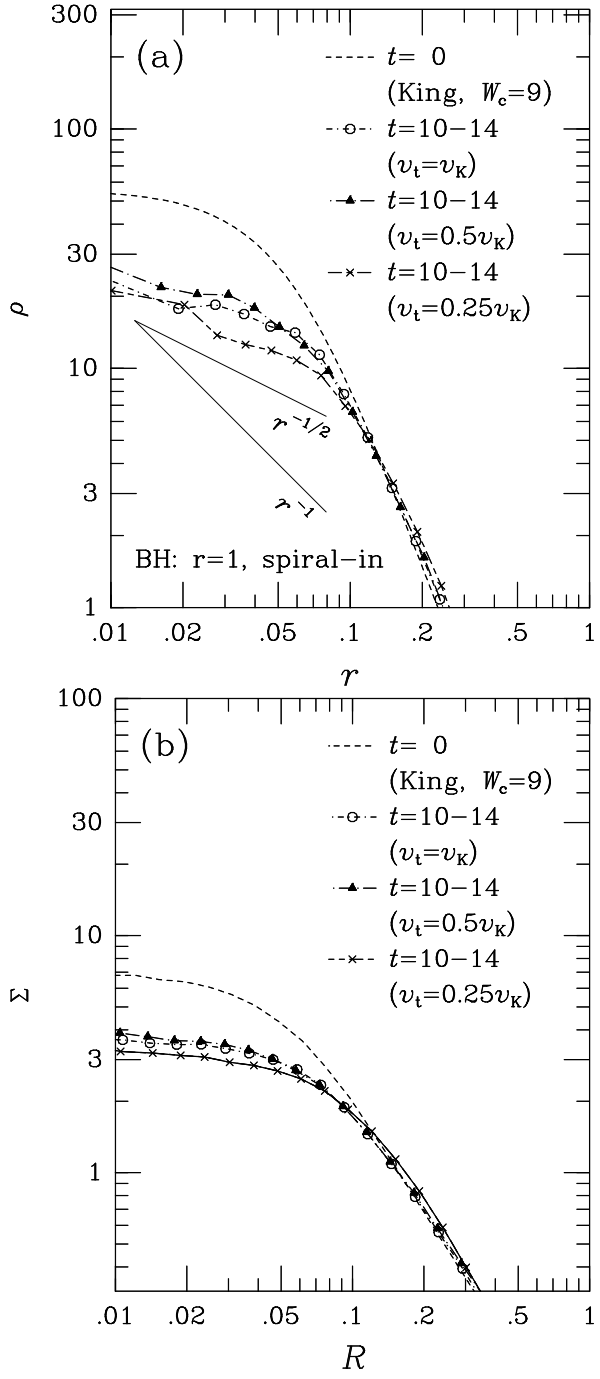

Fig. 4.— (a),(b) Same as Figure 3 but for spiral-in BH (run B, C and D).

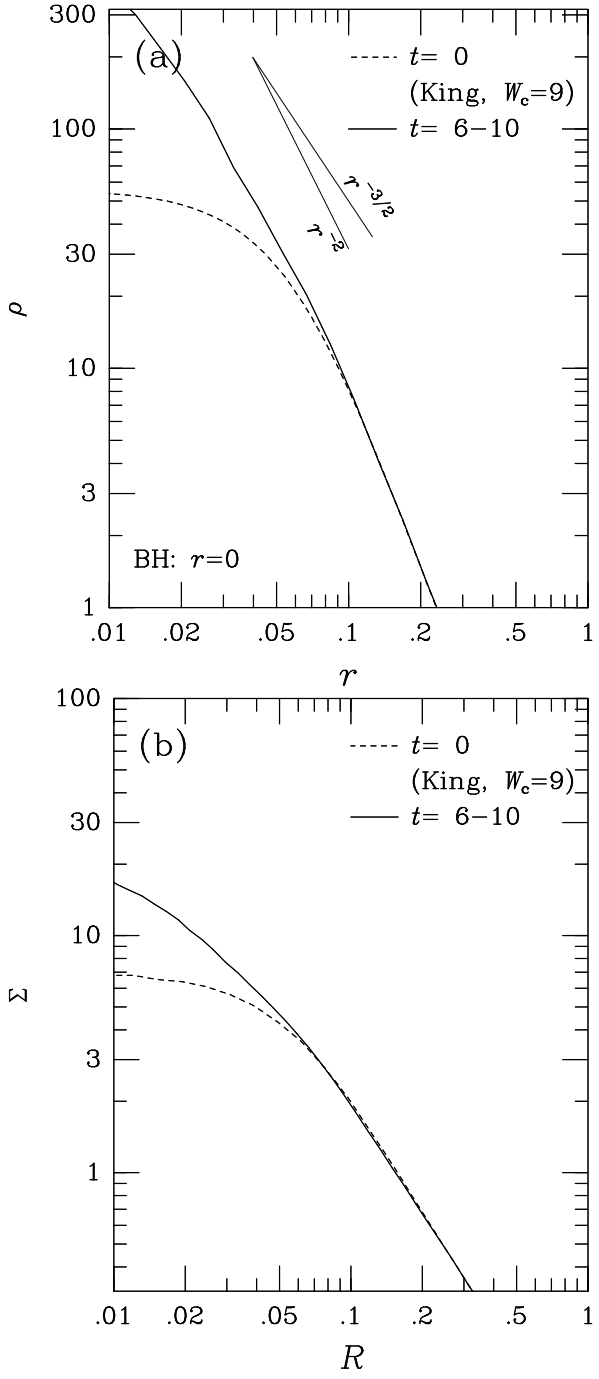

Fig. 5.— (a),(b) Same as Figure 3 but for on-center BH (run E).

$$\times \left[\left(1 - \frac{R^2}{r_i^2} \right) v_{ri}^2 + \frac{1}{2} \frac{R^2}{r_i^2} v_{ti}^2 \right] \Bigg\}^{1/2}, \quad (3)$$

where $\langle v_r^2 \rangle$ and $\langle v_t^2 \rangle$ are, respectively, the radial and tangential mean square velocities.

In the central region ($r < 0.1$), the velocity dispersion is $\sigma \sim r^{-1/2}$. This is simply because the gravitational potential is dominated by the central black hole. In Figure 7, we can see that the projected one-dimensional velocity dispersion also shows a marked increase at the center. The velocity dispersion profiles are rather similar for off-center run and on-center run, since the central potential is dominated by the black hole in both runs. However, if we compare Figures 7a and 7c closely, it is clear that the central increase of $\sigma_{\rm los}$ is less pronounced in the case of the off-center run (Figure 7a). That is because the density cusp is weaker. The results of the spiral-in runs (Figure 6b and 7b) are almost the same as that of the off-center run, like the result for density profile.

In Figure 8, the velocity anisotropy parameter

$$\beta = 1 - \langle v_t^2 \rangle / 2 \langle v_r^2 \rangle. \quad (4)$$

is plotted against the distance from the center of the galaxy. From this equation, $\beta = 0$, $-\infty$, $+1$ for an isotropic velocity distribution, purely circular orbit, and purely radial orbit, respectively.

Here, the difference between off-center and on-center runs is quite clear.

In run E, the change in the anisotropy is monotonic, and inner region is more radial. This can be interpret as the instantaneous response of stars to the injection of the central black hole. If the central potential suddenly deepens, the orbit becomes more radial. Note that this is quite different from the adiabatic response of orbit studied by Young (1980) and Quinlan et al. (1995). In the case of the adiabatic response, orbits become more circular.

In run A, however, the behavior of the anisotropy is more complex. In the outermost region, orbits are predominantly radial because the stars kicked out by the black hole populate the outer halo. The effect of the black hole explains the general increase in β in the outer region.

However, in the innermost region, β decreased. There are at least two possible mechanisms for this decrease. First, the black hole should have ejected stars with radial orbit more efficiently than those with circular orbit. Second, the increase in mass at the center of the galaxy is not instantaneous as in the case of run E. Therefore, the response of orbits would be somewhere in between increase in β for run E and decrease in β for the adiabatic response. If the response is closer to adiabatic, it is natural that β decreases.

In the spiral-in runs (runs B, C and D), β shows the same tendency as that in the off-center run: β increased in outer region and decreased in inner region. The stars in central region of the spiral-in run are somewhat more circular than those in the same region of run A. Since the black hole deposited the angular momentum to the field stars, this result is quite natural.

Figure 9 shows the distribution of kurtosis, i.e. the fourth moment of the line-of-sight velocity dispersion. We plot the dimensionless kurtosis $\kappa = \langle v_{\rm los}^4 \rangle / \sigma_{\rm los}^4$ against the radius for runs A, B, C, D and E. Here the kurtosis is calculated as follows (Merrifield & Kent 1990):

$$\begin{aligned} \langle v_{\rm los}^4 \rangle (R) &= \frac{2}{\Sigma(R)} \int_R^\infty \frac{dr\, r\rho}{\sqrt{r^2 - R^2}} \\ &\quad \times \left[\left(1 - \frac{R^2}{r^2} \right)^2 \langle v_r^4 \rangle \right. \\ &\quad \left. + 3 \frac{R^2}{r^4} (r^2 - R^2) \langle v_r^2 v_t^2 \rangle + \frac{3}{8} \frac{R^4}{r^4} \langle v_t^4 \rangle \right] \\ &= \frac{1}{2\pi\Sigma(R)} \sum_{i(r_i > R)} \frac{m_i}{r_i \sqrt{r_i^2 - R^2}} \\ &\quad \times \left[\left(1 - \frac{R^2}{r_i^2} \right)^2 v_{ri}^4 \right. \\ &\quad \left. + 3 \frac{R^2}{r_i^4} (r_i^2 - R^2) v_{ri}^2 v_{ti}^2 + \frac{3}{8} \frac{R^4}{r_i^4} v_{ti}^4 \right]. \quad (5) \end{aligned}$$

In these figures, $\kappa = 3$ corresponds to a Maxwellian velocity distribution. Larger values of κ ($\kappa > 3$) imply high-velocity tails, and values of $\kappa < 3$ imply "boxier" distributions.

In all cases, the kurtosis is always less than 3 and decreases toward the center, except in the very central region and in the outer region. This result is consistent with the result for an adiabatic growth BH model by Quinlan et al. (1995).

3.4. Black Hole Mass & Core Radius

Figure 10 shows the time-averaged density profiles for runs A, F and G ($M_{\rm BH} = 0.04, 0.02, 0.08 M_{\rm tot}$) for $t = 6 - 10$. We can see that more massive black holes make larger cusp regions. We can also see that the

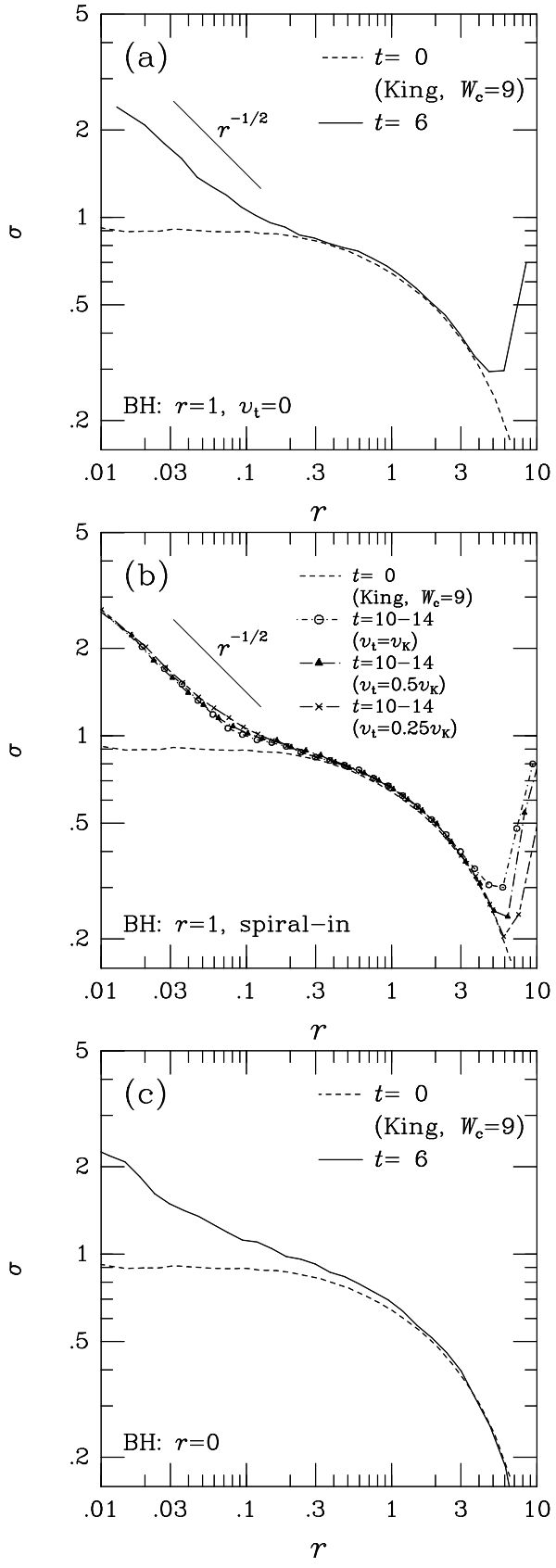

Fig. 6.— Velocity dispersion profiles. (a) for off-center BH (run A); (b) for spiral-in BH (runs B, C and D); (c) for on-center BH (run E).

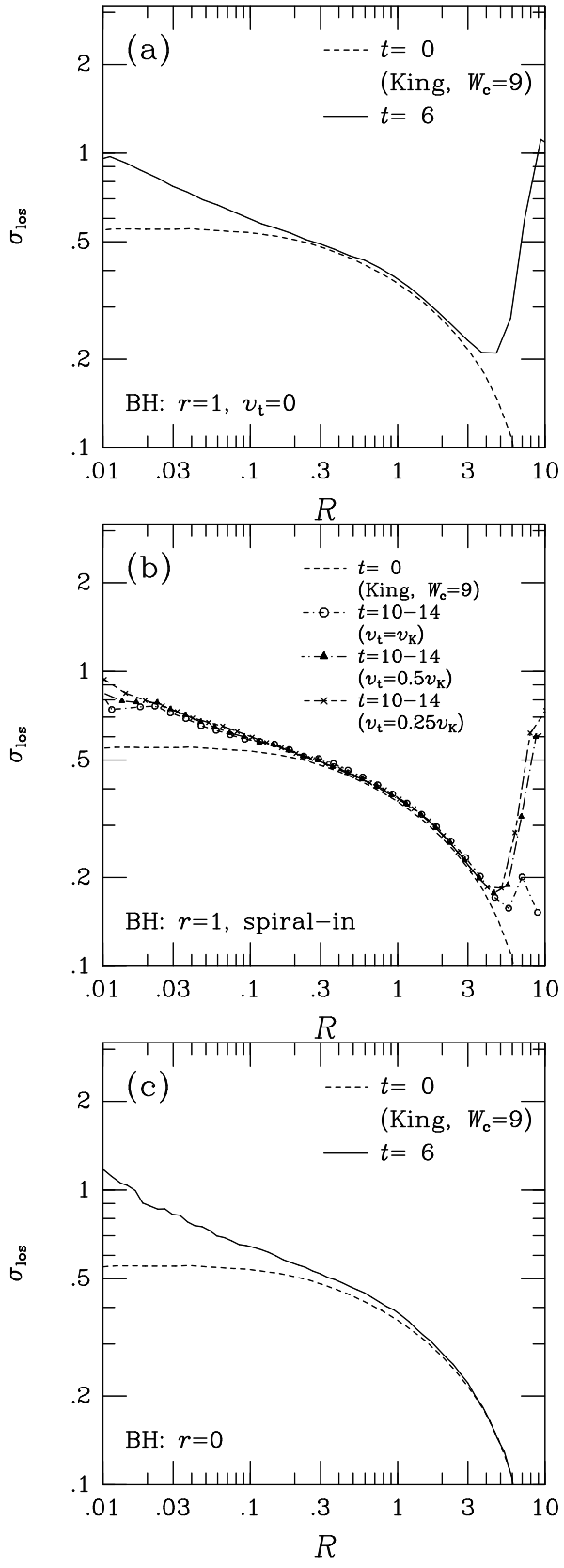

Fig. 7.— Line-of-sight velocity dispersion profiles. (a) for off-center BH (run A); (b) for spiral-in BH (runs B, C and D); (c) for on-center BH (run E).

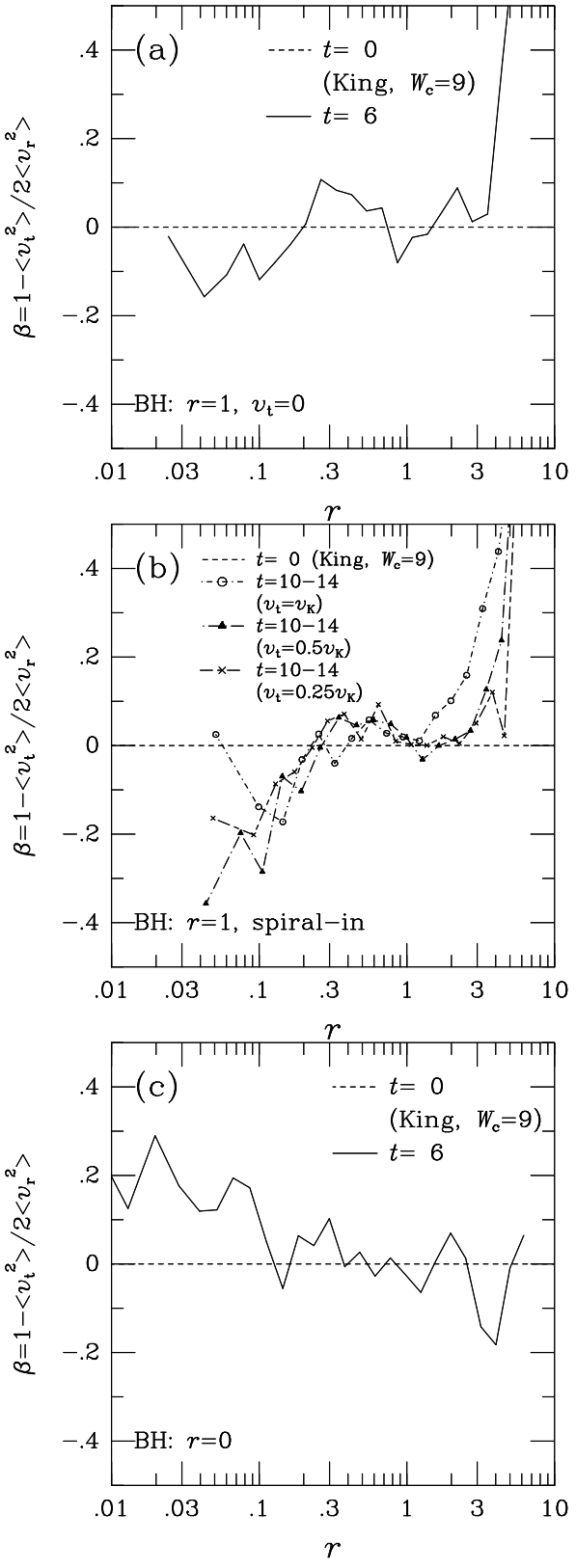

Fig. 8.— Profiles of anisotropy parameter for the velocity dispersion. (a) for off-center BH (run A); (b) for spiral-in BH (runs B, C and D); (c) for on-center BH (run E). Plotted points are the averaged points of the data in logarithmic bins for r. We put 10 bins per decade.

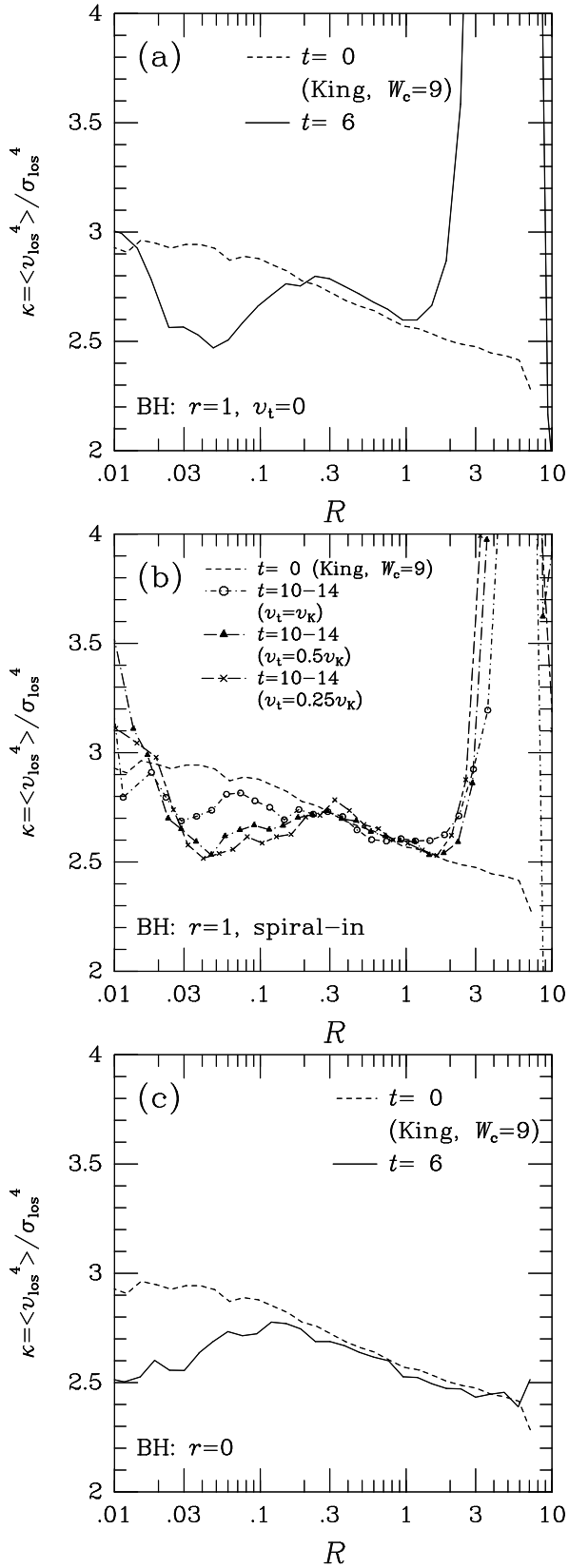

Fig. 9.— Profiles of kurtosis of the line-of-sight velocity. (a) for off-center BH (run A); (b) for spiral-in BH (runs B, C and D); (c) for on-center BH (run E). Plotted points are the averaged points of the data in logarithmic bins for r. We put 10 bins per decade.

slope of the cusp is almost the same for all three runs.

Figure 11a shows the relation between the black hole mass and the "core radius". We adopted the definition of the core radius by McMillan, Hut, & Makino (1990):

$$r_{\rm c} = \sqrt{\frac{\sum_i \rho_i^2 r_i^2}{\sum_i \rho_i^2}}, \qquad (6)$$

where r_i is the distance of star i from the central black hole and ρ_i is the local density at the position of star i. This definition gives a good estimate of the size of the "weak cusp" region (Makino & Ebisuzaki 1996). Figure 11b shows the relation between the black hole mass and the mass of stars within the core radius.

Figures 11a and b indicate that the core size shows almost linear dependence on the black hole mass. Of course, the relation is not strictly linear simply because the initial King model had a finite core. Even for zero black hole mass the core size is still finite.

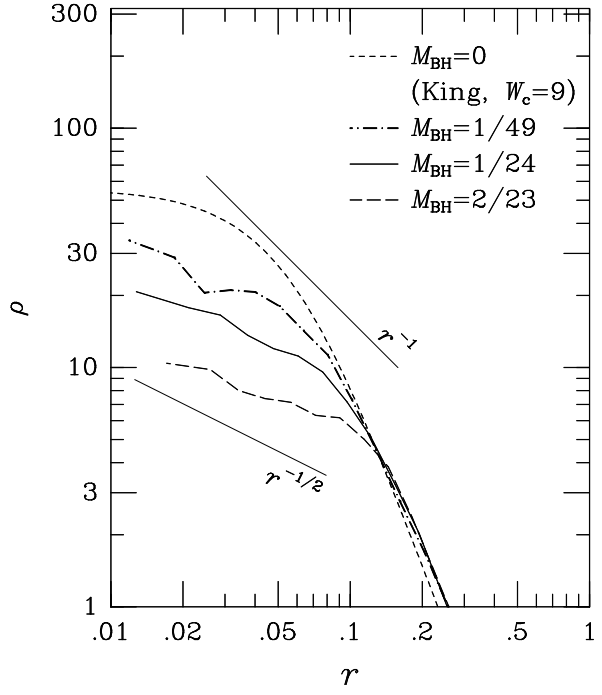

Fig. 10.— Density profiles for BH mass $M_{\rm BH} = 1/49, 1/24$ and $2/23$ (run F, A and G), respectively.

3.5. Dependence on the Galaxy Model

Figure 12 shows the time-averaged density profile for $t = 20 - 24$ for run H and $t = 40 - 44$ for run I. We used less concentrated King model ($W_{\rm c} = 6, 3$) as

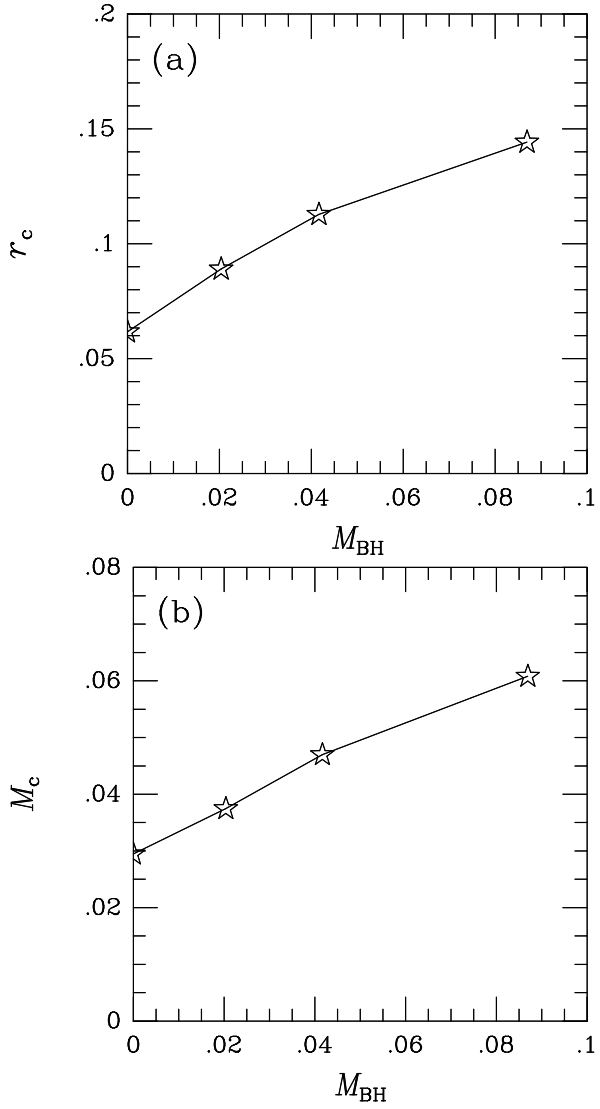

Fig. 11.— (a) Relation between the BH mass $M_{\rm BH}$ and core radius $r_{\rm c}$ for the run F, A and G, respectively. (b) Relation between the BH mass $M_{\rm BH}$ and core mass $M_{\rm c}$ for the run F, A and G, respectively.

initial galaxy models for these runs. It has the core about 10 times larger than that of the model we used for all other runs. The result of run H (figure 12a) shows that the structure of the core remains almost unchanged. The result of run I (figure 12b) shows that the flat core is replaced by a slight increase in the central density ($\rho \propto r^{-0.3}$). However, in this run, the initial potential energy of the black hole is not much larger than the bound energy of the stars in the core, since the core size is as large as the initial distance of the black hole from the center of the galaxy. Therefore, this "cuspy" profile is likely to be formed through the process similar to that for run E, when we placed the black hole in the core.

3.6. Effect of Two-Body Relaxation

Figure 13 shows the time evolution of the density profile for runs with different number of particles (runs A and J). All other parameters are the same. In Figure 13a, it is clear that the central cusp becomes steeper as the system evolves, while in Figure 13b (run J) the change is negligible. This difference is due to the difference in the thermal relaxation time. The model in run A has much shorter relaxation time. Real galaxies have the relaxation time several orders of magnitude larger than that of the model in run J. Therefore, in real ellipticals the thermal evolution would be negligible and the profile would not change.

4. Discussion and Summary

We investigated the dynamical effect of a massive black hole which sinks into the galactic center to the structure of the galaxy by means of N-body simulations. We obtained three main results.

First, we found that the black hole destroys the central core of the initial galaxy by heating up the field stars. After the black hole settled in the center, a weak density cusp ($\rho \sim r^{-0.5}$) remained around the central black hole. This result does not depend on how much angular momentum the sinking black hole initially has. This result nicely explains the recent *HST* observations of large elliptical galaxies (Lauer et al. 1995; Byun et al. 1996; Gebhardt et al. 1996; Faber et al. 1996; Kormendy et al. 1996). On the other hand, when a massive black hole is placed initially at the galactic center, the central density increases and a steep cusp ($\rho \propto r^{-1.5}$) is formed.

Second, the velocity anisotropy profiles are quite different between the above two cases. For the off-

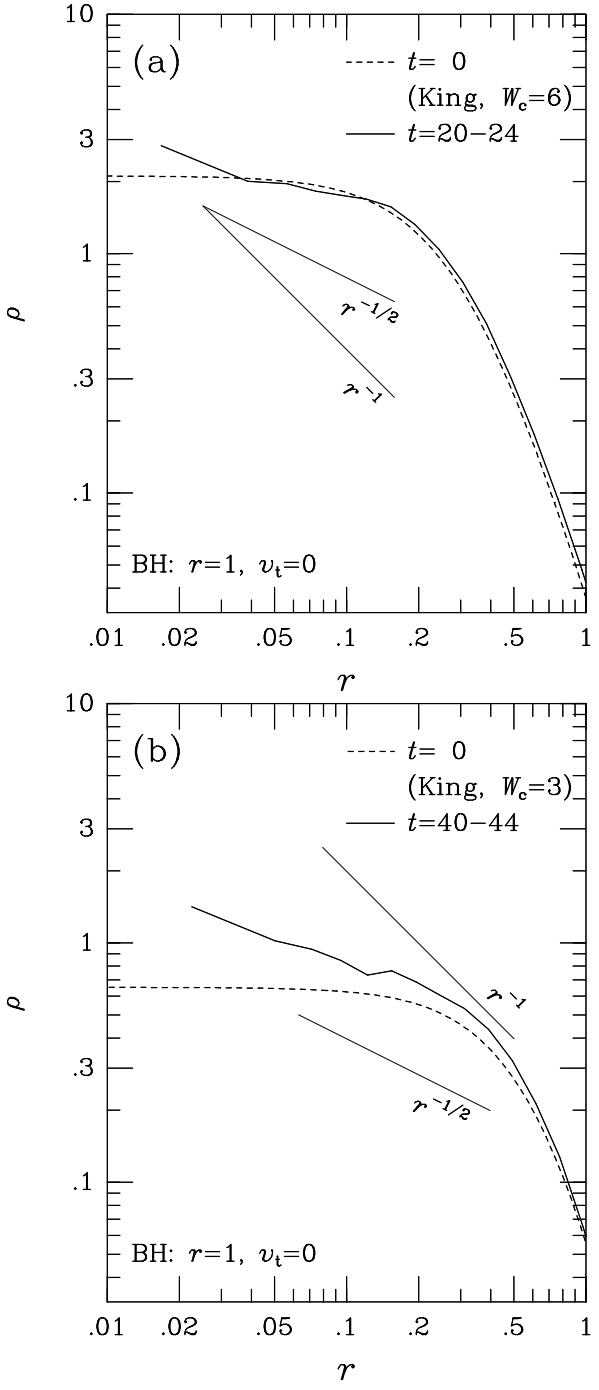

Fig. 12.— (a) Density profile for King model with $W_c = 6$ (run H). (b) Same as (a) but for King model with $W_c = 3$ (run I).

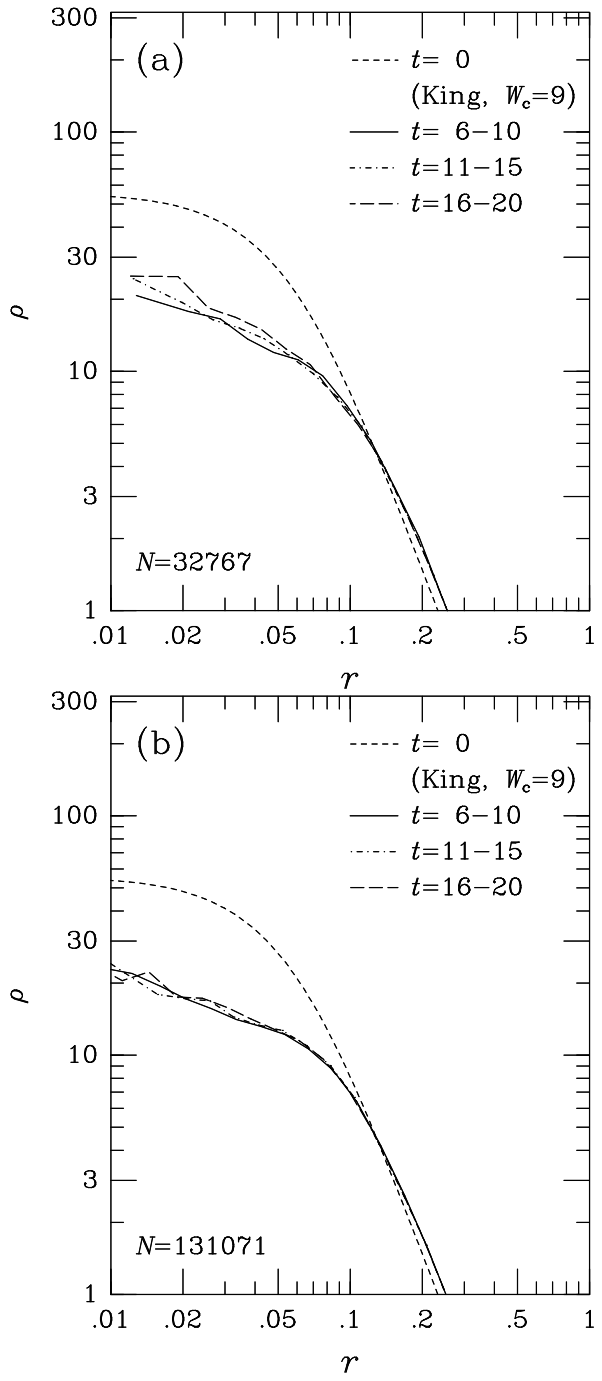

Fig. 13.— (a) Time evolution of density profile for $N = 32767$ (run A). (b) Same as (a) but for $N = 131071$ (run J).

center black hole model, the orbits of the stars in the outer region tend to be radial, while in the inner region, the orbits tend to be circular. If the black hole spirals into the center, the field stars get angular momentum from the black hole and the orbits become more circular in the innermost region. For the on-center black hole model, however, the velocity is more radial near the center and approximately isotropic in the outer region.

Third, the size of the weak cusp region shows a clear correlation with the black hole mass. The heavier black holes form larger cores.

From the present results, we can conclude that the weak density cusp can be formed if a massive black hole dynamically sinks to the center of a galaxy. This suggests that the prime cause of the formation of the weak cusp in simulations by ME is the back reaction to the sinking black holes. Moreover, the origin of the weak cusp in large elliptical galaxies found with recent *HST* observations can be explained by this galaxy merging and subsequent sinking of black holes. From this point of view, the dichotomy of elliptical galaxies ("core" galaxies and "power-law" galaxies (Lauer et al. 1995; Byun et al. 1996; Gebhardt et al. 1996; Faber et al. 1996; Kormendy et al. 1996)) could be understood as follows: small and therefore "cuspy" ellipticals and normal spirals are most likely to be formed through dissipational collapse. During the formation process, they are likely to contain moderately massive central black holes ($\sim 10^7 M_\odot$). When these galaxies merge, black holes spiral into the center of the merger and left the weak cusp. If the merger still contain gas, significant fraction of that mass would accrete to the black hole (Taniguchi & Wada 1996). In this process, "cuspy" profile might be restored. However, if gas is already consumed by some process, the weak cusp is preserved. Thus, massive ellipticals are likely to have weak cusps, while less massive ones are likely to have deep cusps, even if they are mergers.

In addition, we investigated the possibilities of identifying the mechanisms of the formation of the central cusps in elliptical galaxies by comparing our results with the observations. We calculated the line-of-sight velocity dispersion and the kurtosis for both models, but the difference in the profiles of them are quite small. There was a clear difference in the anisotropy. However, to determine anisotropy from observation is not easy. Thus, it will be very difficult to detect the difference of the two types of the cusps in the spectroscopic data. The most clear differ-

ence is in the density profile. If the improved velocity dispersion data for the observed "weak-cusp" galaxies demonstrates the presence of massive black holes, our scenario would be the most plausible explanation.

We thank Yoko Funato for helpful comments on the simulation method and the manuscript. We are grateful to Shunsuke Hozumi for valuable conversations and for his comments on previous drafts of this paper. T.N. thanks Toshiyuki Fukushige for much useful advice on the calculation method and for stimulating discussions. We also thank Daiichiro Sugimoto and all the people who developed the special-purpose computer GRAPE-4.

REFERENCES

Aarseth, S. J., 1985, in Multiple Time Scales, ed. J. U. Brackbill & B. I. Cohen (Orlando: Academic), 377

Bahcall, J. N., & Wolf, R. A., 1976, ApJ, 209, 214

Byun, Y., et al., 1996, AJ, 111, 1889

Faber, S. M., et al., 1996, AJ(submitted)

Fukushige, T., & Makino, J., 1997, ApJ, 477, L9

Gebhardt, K., et al., 1996, AJ, 112, 105

Heggie, D. C., & Mathieu, R, D., 1986, in Lecture Note in Physics, 267, The Use of Supercomputers in Stellar Dynamics, ed. P. Hut & S. McMillan (Berlin: Springer), 233

Kormendy, J., 1985, ApJ, 292, L9

Kormendy, J., et al., 1996, in IAU Symp. 171, New Light on Galaxy Evolution, ed. R. Bender & R. L. Davies (Dordrecht: Kluwer), 105

Lauer, T. R., 1985, ApJ, 292, 104

Lauer, T. R., et al., 1995, AJ, 110, 2622

Makino, J., & Aarseth, S. J., 1992, PASJ, 44, 141

Makino, J., & Ebisuzaki, T., 1996, ApJ, 465, 527

Marchant, A. B., & Shapiro, S. L., 1979, ApJ, 234, 317

Marchant, A. B., & Shapiro, S. L., 1980, ApJ, 239, 685

McMillan, S., Hut, P., & Makino, J., 1990, ApJ, 362, 522

Merrifield, M. R., & Kent, S. M., 1990, AJ, 99, 1548

Navarro, J. F., Frenk, C. S., & White, S. D. M., 1996, ApJ, 462, 563

Quinlan, G. D., Hernquist, L., & Sigurdsson, S., 1995, ApJ, 440, 554

Shapiro, S. L., & Marchant, A. B., 1978, ApJ, 225, 603

Taiji, M., Makino, J., Fukushige, T., Ebisuzaki, T. & Sugimoto, D., 1996, in IAU Symp. 174, Dynamical Evolution of Star Clusters, ed. P. Hut & J. Makino (Dordrecht: Kluwer), 141

Taniguchi, Y., & Wada, K., 1996, ApJ, 469, 581

Young, P., 1980, ApJ., 242, 1232

This 2-column preprint was prepared with the AAS LaTeX macros v4.0.